LA-UR-13-24376
Approved for public release; distribution is unlimited.

Title: AOT & LANSCE Focus: Proton Radiography Facility

Author(s): Kippen, Karen E.
Fulton, Robert D.
Brown, Eric
Buttler, William T.
Clarke, Amy J.
Kwiatkowski, Kris K.
Mariam, Fesseha G.
Merrill, Frank E.
Morris, Christopher
Olson, Russell T.
Zellner, Michael

Intended for: Marketing material

Issued: 2013-06-14

AOT&LANSCE FOCUS

PROTON RADIOGRAPHY FACILITY

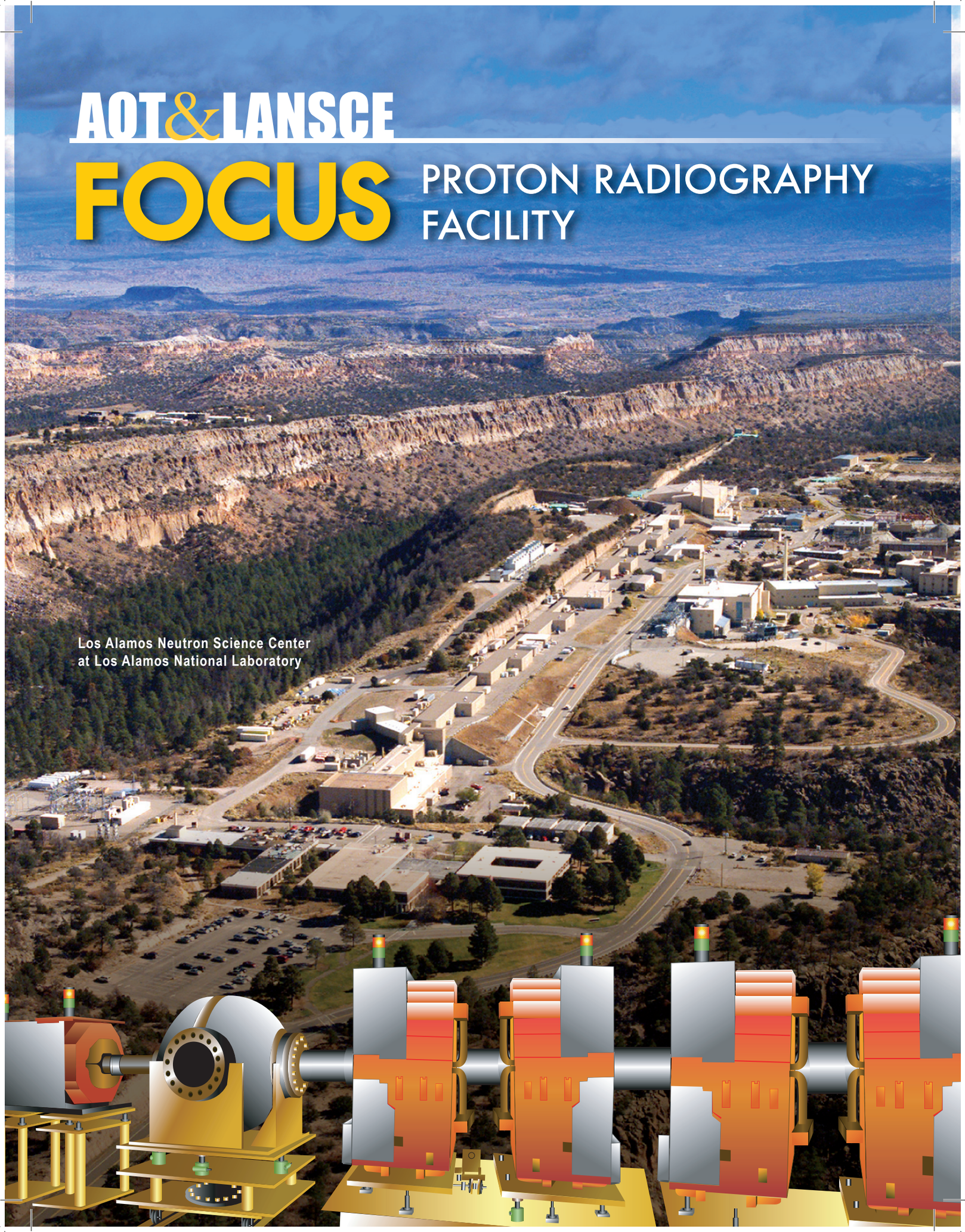

Los Alamos Neutron Science Center
at Los Alamos National Laboratory

pRad at Los Alamos National Laboratory

Invented at Los Alamos National Laboratory, proton radiography (pRad) at the Los Alamos Neutron Science Center (LANSCE) employs a high-energy proton beam to image the properties and behavior of materials under a variety of conditions. The penetrating power of high-energy protons, like that of x-rays, makes them an excellent probe of a wide range of materials under extreme pressures, strains, and strain rates. The invention of proton radiography is the direct result of the synergy between the Laboratory's defense mission and basic science research scientists and supports the Laboratory's national security science mission as well as provides for fundamental science discoveries. This new capability has revolutionized dynamic materials science at Los Alamos, providing a new window for the study of shock physics, materials damage, and high explosives science. The Proton Radiograpy Facility, a national user facility, has performed more than 500 dynamic experiments in support of the Weapons program, Global Security, and other customers since it was commissioned more than a decade ago. This information helps Los Alamos maintain the reliability of the U.S. nuclear stockpile. The pRad capability is primarily supported by the NNSA Science Campaigns.

Utilizing the 800-MeV proton beam generated by the LANSCE linear accelerator, the efficacy and versatility of proton radiography stems from the ability to produce multiple proton pulses in an accelerator coupled with multiple optical viewing systems that can result in 42-frame movies in a dynamic event with frames separated by 200 nanoseconds. Two radiography systems can be used at the facility: the identity lens system provides a ~120-mm field of view with ~180-micron resolution; the second system magnifies the proton image, providing ~60-micron resolution over a 40-mm field of view. Both systems are capable of radiographing experiments that have up to 50 g/cm^2 of line-integrated density through the object. This corresponds to approximately 2.5 centimeters of uranium or 20 centimeters of aluminum. Absolute densities can typically be measured to better than 5%, while relative densities can be measured to better than 1%. The LANSCE linear accelerator provides considerable timing flexibility for both dynamic and quasi-static experiments. Data at rates up to 10 Hz can be taken for both tomographic applications or for experiments with slower dynamic evolution.

The majority of experiments are performed using high explosives as material drivers, however, a variety of dynamic drivers are available, including a powder gun that accelerates a 40-mm-diameter flyer plate up to ~2 mm/μs. These experiments are performed in a 6-foot-diameter vessel with 2-inch-thick steel walls, capable of containing dynamic experiments with up to 10 pounds of high explosives. Nearly all materials can be studied with this proton radiography system, although some hazardous materials require additional mitigation for use.

Doug Fulton
Physics Division Leader

On the cover: **An aerial view of the 800-MeV LANSCE proton accelerator with an illustration of the pRad focusing magnet system and containment vessel.** ***Next page:*** **A view from above—the pRad focusing magnets and imaging station (bottom of the photograph).**

AOT & LANSCE FOCUS

PROTON RADIOGRAPHY FACILITY

Colleagues,

This is a special *Pulse* issue focusing on the Proton Radiography (pRad) Facility at LANSCE. The pRad facility is one of the three DOE-designated user facilities at LANSCE addressing NNSA's mission and fundamental research. This unique experimental capability, combined with an excellent and dedicated team of technical and scientific leaders from across the Laboratory, is poised to continue making mission relevant and fundamental discoveries into the future.

Alex Lacerda,
LANSCE Deputy Division Leader

pRad at work

pRad into the future

Acknowledgments: This work was performed under the auspices of the U.S. Department of Energy under Contract DE-AC52-06NA25396.

Physics and technology of proton radiography

Lens-focused proton radiography, invented in 1996, has been developed as a multipulse, flash radiography technique. The longer mean free path of high-energy protons provides a more penetrating probe, well suited to hydrotest radiography. Since its invention in the mid-1990s charged particle radiography has been extensively developed. The results of this work and its many advantages are reviewed in the following section.

An alternative to x-radiography is provided by protons. In contrast to x-rays, protons are charged particles. Although protons of sufficient energy can be transmitted through matter, they continuously interact with the electrons and nuclei in the matter. These interactions consist of the Coulomb interaction between the beam and the electrons, the Coulomb interactions between the beam and the nuclei, and the nuclear interaction of the protons and the atomic nuclei. To a good approximation these can be treated separately and each can be used for radiography.

The Coulomb interaction with the much lighter electrons results in continuous energy loss and eventual stopping of the protons. The stochastic nature of proton electron scattering, which results in a distribution of energy loss that depends on the material thickness, is described by Landau and Vavilov. For stopped protons this results in a distribution of ranges. The Coulomb interaction between protons and atomic nuclei results in deflections of the proton trajectory, but negligible energy changes. Because the integral of the Coulomb cross section is infinite, the solution to the problem of charged particle transport in matter is nontrivial. The number of collisions is large and this process results in a continuous increase of the angular divergence of the beam described by Coulomb multiple scattering.

The cross sections for nuclear scattering are relatively small, therefore fluctuations induced by nuclear scattering are determined by a smaller number of collisions than either of the Coulomb processes. To a good approximation, nuclear scattering can be separated into elastic (small energy loss) and inelastic (large energy loss pieces).

The earliest use of protons for radiography showed that by range straggling (marginal range radiography) high contrast radiographs could be made with low doses, but with poor spatial resolution when compared with x-rays. A number of studies followed this initial work, demonstrating the potential of proton radiography for biological and other nondestructive applications.

Hanson et al. showed that better position resolution could be obtained by measuring the energy of transmitted protons in a calorimetric detector (energy loss radiography)—essentially ranging out the protons in the detector. This technique resulted in the same small doses and high contrast—but obtained better position resolution by using higher energy protons and minimizing multiple scattering.

Coulomb multiple scattering results in interesting phenomena. Protons have a tendency to pile up along the interface between materials with different Coulomb scattering densities. Protons scatter out of high density material with greater probability than they scatter back in, highlighting the edges at material interfaces. Later, nuclear scattering was used to produce 3D images of objects by tracking both the incident and the scattered beam.

Proton mean free path

The absorption cross section, σ_A, for hadrons on a nucleus with mass number A is well approximated by $\sigma_A = \pi r_A^2$, the geometric cross section of the nucleus, where $r_A \approx 1.2A^{1/3}$ fm. Using $\lambda = 1/\rho\sigma$ gives an estimate of the hadronic mean free path in uranium of 220 g/cm^2. This is within 11% of the tabulated value of 199 gm/cm^2.

Multiple scattering radiography

In proton radiography two components contribute to the attenuation, $t = t_\lambda t_c$, where t is the total transmission. The first term is due to nuclear scattering/absorption and the second is due to Coulomb multiple scattering. Proton radiography relies on magnetic lenses to restore position resolution lost due to the Coulomb multiple scattering. The ratio of images in a two lens proton radiography system can separate the loss of flux due to multiple scattering from the nuclear attenuation loss. If the multiple scattering angular distribution is given by a Gaussian, the transmission through an aperture, θ_c, for an object of thickness, z, is given by:

$$t_c = (1 - e^{-\frac{\kappa}{z}}) \qquad 1)$$

where:

$$\kappa = \frac{\theta_c^2 p^2 \beta^2 \mathrm{X}_0}{(14.1\ \mathrm{MeV})^2}$$

Here θ_c is the angular acceptance of the lens, p is the proton momentum in units of MeV/c, β is the proton velocity in units of the velocity of light, and X_0 is the radiation length in the same units as z. The length scale κ for multiple scattering radiography can be chosen by using an angle collimator at a Fourier point in the magnetic lens to select θ_c. An optical analog is an aperture to select angles in a telecentric lens.

An error analysis can be performed by taking the derivative of eq 1) with respect to z:

$$\frac{dt_c}{dz} = \frac{\kappa}{z^2} e^{-\frac{\kappa}{z}}. \qquad 2)$$

pRad contributions to weapon physics

This has been another good year for pRad (proton radiography) contributions to the weapons program. pRad provides a unique, many-frame, sub- microsecond imaging and densitometry of weapon hydrodynamics, with the real weapon explosives and materials (or appropriate surrogates). The time range, number of frames and accuracy of density gradient determination, and shock location, is unmatched by any other diagnostic facility, with thick object penetration sufficient for high value scaled implosion experiments. The multi-frame, time resolved data continues to prove extremely valuable for hydro-code validation of detailed, anomalous flows.

This last year, we've had an impressive data return from pRad experiments, ranging from HE Initiation, detonation wave propagation and accurate dead zone measurements for insensitive high explosives, required from the DSW program, to measurements of surface ejecta and multi-material mixing under shock loading. A number of novel HE experiments were successfully executed that clearly support options for pit reuse under consideration. These experiments once again demonstrated the creativity and ingenuity of the scientific workforce at Los Alamos National Laboratory in support of the stockpile mission. Phenomenal results from the Richtmeyer-Meshkoff interface instabilities under HE drive experiments provided data needed to develop new models of ejecta formation which will provide a yet deeper physical basis for our stockpile stewardship efforts. In view of these accomplishments, the pRad team has once again earned thanks from the weapons program.

Robert B. Webster
Associate Director Weapons Physics

The relative uncertainty in the measurement of z is:

$$\frac{\Delta z}{z} = \frac{z}{\kappa}\frac{\sqrt{t_c}}{1-t_c}\frac{1}{\sqrt{N_0}} \qquad 3)$$

where the uncertainty in the measurement of transmission is again assumed to be due to counting statistics. Equation 3) can be solved for a minimum as a function of κ. The result is $\kappa = 0.644\ z$. The relative size of the uncertainty for a given incident flux is about a factor of 1.5 larger than for transmission radiography. In addition, the size of the error grows rapidly as z/κ gets smaller but grows more slowly as z/κ gets larger, the opposite of the behavior of pure attenuation radiography.

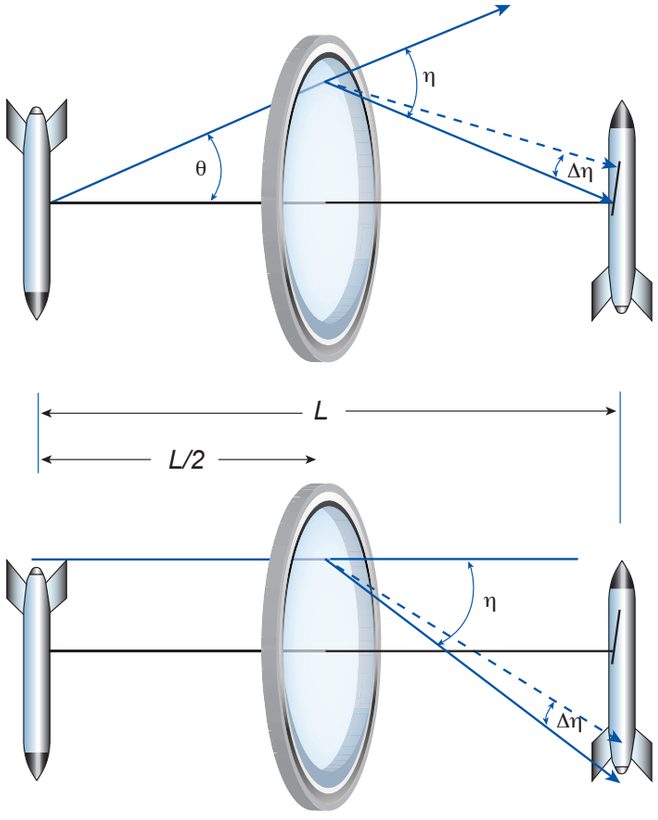

Figure 1. Schematic drawing of a symmetric (-I) lens. Here η=2θ is the change in angle produced by the lens at the focus momentum and Δη is the change in bending angle produced by chromatic aberrations.

Charged particle lenses

The multiple scattering of charged particles when they pass through matter leads to position blur. The blur due to drift space after the object is proportional to the drift length and the multiple scattering in the object. A simple focusing lens deflects particle trajectories by an angle proportional to their radial distance from the axis. Although the only implementations of such a lens, e.g., solenoid, electrostatic, or lithium lenses, are not suitable for high-energy charged particle radiography (they are not strong enough or they introduce material into the particle trajectories), a simple model based on them has provided the guidance leading to the magnetic systems currently used for charged particle radiography.

A lens producing an angle change of $\Delta\theta = kr$, where r is the distance from the axis and k is a constant, produces a unit magnification focus at $L=1/k$, where $L/2$ is the distance between the center of the lens and the object and image planes. Figure 1 shows a schematic drawing of such a lens. If this lens is illuminated with parallel rays, the acceptance of the lens is a function of position, much like was observed with the quadrupole doublet lens used in Figure 2. However, if the illuminating beam has a position angle correlation built into it so it is aimed to a point on the axis at the center of the lens, this position angle correlation is removed. In this case, the angular acceptance is uniform across the object plane and scattering of the incident beam is imaged in the plane of the lens. Both of these are important features of a lens for proton radiography.

An additional feature of the position angle correlation built into the illuminating beam is the cancellation of the lowest order aberrations of a magnetic lens, which has a momentum dependent focus. The bending angle of a charge particle in a magnetic field is proportional to $1/p$ where p is the particle's momentum. Because of this, k depends on momen-

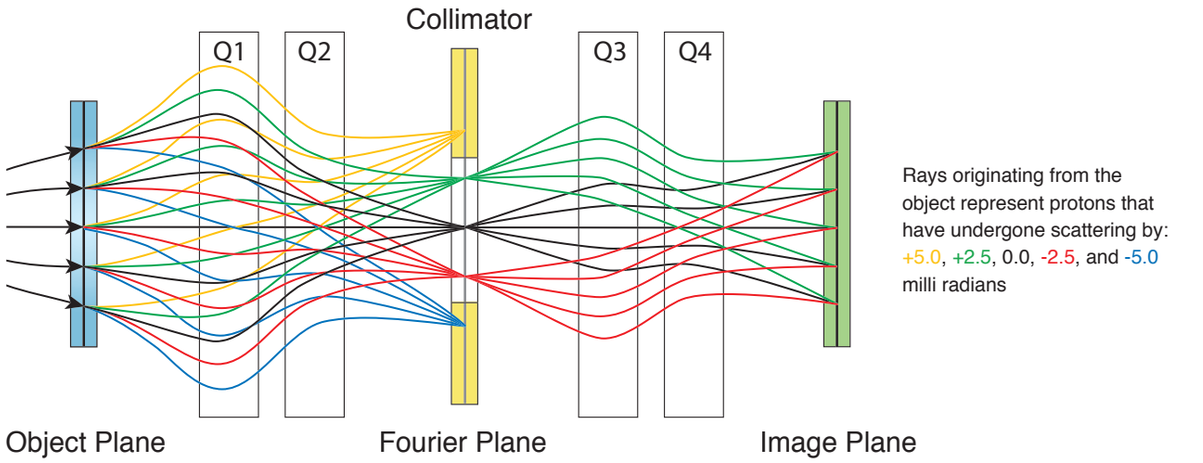

Figure 2. A COSY rendition of the x1 magnetic imaging lens made up of quadrupole electromagnets Q1, Q2, Q3 and Q4. The incoming proton beam is arranged as indicated by the black arrows, where the direction of the protons is correlated to its position with respect to the optical axis of the quadrupoles. This is the matching condition discussed in the text. For a beam arranged in such manner, the protons are sorted into radial positions at the Fourier Plane; the radial position depends only on the angular deflection suffered by the proton due to Coulomb scattering at the "object." Placing an aperture restriction (collimator) at the Fourier plane, removes protons that have scattered through large angles. As indicated in the text, use of small collimators leads to enhanced resolution.

tum. The upper part of Figure 1 shows the consequence of this for an off momentum trajectory.

The coordinates of a particle in the image plane (x',θ') can be expressed in terms of the initial coordinates (x',θ') as:

$$x' = R_{11}x + R_{12}\theta \qquad 4)$$
$$\theta' = R_{22}\theta + R_{21}x$$

The matrix $\boldsymbol{R}$ has a determinate of -1. For unit imaging R_{11}=-1 and R_{12}=0, so R_{22}=1. If this analysis is carried to higher order for a lens that is chromatic, the expression becomes: $x' = x + T_{116}x\delta + T_{126}\theta\delta$

where $\delta = \dfrac{p - p_0}{p}$

is the fractional deviation of the transmitted momentum from the momentum the lens is set to focus, p_0. As can be seen from simple geometry, T116=2 and $T_{126}=L$ are the coefficients in the Taylor series expansion of the chromatic aberrations for the lens depicted in Figure 1. The chromatic length of the lens is $L_{ch}=T_{126}$. By building in a correlation in the illuminating beam,

$$\theta = \frac{T_{116}}{T_{126}}x \qquad 5)$$
$$= \frac{2x}{l}$$

chromatic aberrations are cancelled to lowest order. This is exactly the angle-position correlation leading to uniform acceptance and angle sorting in the lens plane. A simple symmetric quadrupole lens with angle matching solved the acceptance issues of the first lens focused imaging experiments, with the added benefit of eliminating effects of lowest order chromatic aberrations.

Magnetic quadrupole lens

Mottershead and Zumbro have realized these conditions for a lens constructed from magnetic quadrupole magnets. Although the basic principles are similar to the simple optical analog presented previously, magnetic quadrupole lenses are more complicated. Remarkably, the cancellation of chromatic aberrations accomplished by the "matching" of the angle-position correlation of the beam using the second order transport properties of the lens results in angle sorting a Fourier plane located at the center of the lens, just as in the simple case above.

Figure 2 is a schematic layout of one of the unit magnification (-I) lenses used at the Proton Radiography (pRad) Facility at the Los Alamos Neutron Science Center (LANSCE). Also shown in Figure 2 are the incoming "matched" rays generated using the beam-optics code COSY. At the Fourier plane, scattered protons are sorted into radial positions proportional to their polar scattering angle in the object plane. The contrast for a given

object can be adjusted by adjusting the collimator angle and can be optimized for statistical precision as described by equation 1.

The angle matching has been achieved by using COSY to find linear combinations of changes to the matching quadrupole strengths that move the x and y Fourier points along the z-axis independently. These were adjusted to produce the minimum spot size of an image at the center of the collimator.

Spatial resolution proton radiography

The resolution in proton radiography is a bit more complex than in x-ray radiography because of the lens focusing and the charged particle transport. The spatial resolution has three contributions: chromatic aberrations, blur due to angular and position diffusion in the object, and camera resolution. The chromatic blur function from the lens is approximately Gaussian with a width that is given by:

$$\sigma_{\mathrm{lb}} = L_{ch}\frac{\Delta p}{p}\sigma_\theta \qquad 6)$$

Where

$$\sigma_\theta = \frac{14.1}{p\beta}\sqrt{\int \frac{\rho(x,y,z)}{X_0(x,y,z)}dz} \qquad 7)$$

The Gaussian is convolved with the transmission over the angular acceptance of the lens:

$$T'(x,y) = \int T(x+u,y+u)e^{-\frac{(u^2+v^2)}{2\sigma_\theta^2 L_{ch}^2\delta^2}}du\,dv \qquad 8)$$

where the integral is limited to a circle, $u^2+v^2<\theta_{cut}L_{ch}\delta$, where θ_{cut} is the angular acceptance of the lens. Here T is the unblurred transmission, T' is the blurred image, $L_{ch}=T_{126}$ is the chromatic length of the lens,

$$\delta = \frac{p-p_0}{p_0}$$

where p is the transmitted proton momentum and p_0 is the momentum the lens is set to focus. Neri and Walstrom report a simple model of chromatic aberrations where the integral over the collimator aperture is approximated by a Gaussian with the same angular acceptance. Schach von Wittenau et al. report detailed Monte Carlo calculations of image blur at 800 MeV due to lens transport yielding results similar to these analytic models.

There is also a contribution to the blur function from scattering in the object, which is Gaussian with a width given by:

$$\sigma_{ob}^2(x,y) = \int_0^{z_{\max}} z^2\frac{\rho(x,y,z)}{X_0(x,y,z)}dz \qquad 9)$$

Here the integrand is the radiation length density, and the integral starts at the image plane, z=0, and integrates over the downstream material, z_{max}. To first order there is no blur from material upstream of the image plane. This blur function also needs to be convolved with the transmitted image. In the model here, this convolution is assumed to be independent of the angular acceptance of the lens, giving a small overestimate of the blur.

All of these effects have been incorporated into a forward model of proton radiography where the calculated blur function is numerically integrated over the acceptance of the angular collimator. This is similar to the model described by Walstrom.

Magnifier lens systems

If the lens system shown in Figure 1 is moved closer to the object, as shown in Figure 3, a magnified image can be produced. Experiments that are scale (S) independent can benefit from magnification. As the dimensions of an experiment are scaled down, both the fractional momentum spread and the angular divergence are re-

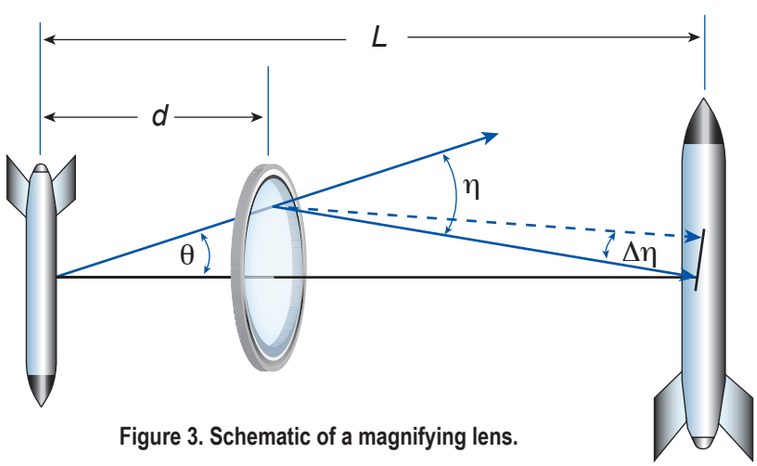

Figure 3. Schematic of a magnifying lens.

duced. The product varies as $S^{3/2}$. Simply mapping the field of view to the new object scale results in a net improvement in the position resolution contribution to the figure of merit (FOM) that goes as $S^{-1/2}$. As the scale is reduced the aperture needed for the lens also deceases. The field strength of magnetic lenses is determined by the magnetic field at the pole tip, which is limited by the saturation field for ion base magnets or by the remnant field for superconducting magnets. As the scale factor is reduced and the magnification is increased, the chromatic length, $L_{ch}=T_{126}/M$, of the lens system is also reduced. Using the optical analog for illustration purposes:

$$\Delta x_{Object} = \Delta\eta(L-d)/M \qquad 10)$$

$$M = \frac{(L-d)}{d}$$

$$\eta = \theta\left(\frac{L}{L-d}\right),\ \ \Delta\eta = \delta\ \theta\left(\frac{L}{L-d}\right),$$

$$\Delta x_{Object} = \frac{\delta\theta L}{M}$$

The first magnetic magnifier was built from neodymium iron permanent magnet quadrupole (PMQ) to reduce the cost compared to electromagnets. It was designed to produce a magnification of 7 and use the same image planes location that was already implemented in the unit imagers in the LANSCE radiographic system. In initial tests, this system worked remarkably well, producing a position resolution of 17 μm. Because of the large magnification and small field of view, this system has not been used for dynamic experiments, but demonstrated many of the features and design philosophy employed in later magnifier designs.

A magnifier with a magnification of ×2.7 has been used for many of the experiments described in the following articles. This system routinely provides better than 100-μm position resolution (as good as 60 μm) with a rectangular object plane field of view of 4 × 4 cm^2. Focusing is accomplished by moving the three downstream magnets on precision-stepping motion-controlled linear stages. One problem encountered with this system is radiation-induced demagnetization of the permanent magnet material. The magnets require repolarization after being used in experiments such as tomography, which require high proton dose.

Yang et al. have presented a design study of a class of magnifiers they call "lengthened lens," which they compare to unit imaging lenses. This class of lenses inherits many benefits of the Zumbro design, while reducing chromatic blur.

Detectors

Proton radiography requires detectors that convert proton fluence in the image plane of a magnetic lens to digitized images. In the case of single proton pulses, technologies such as film or image plates can be used as well as optically shuttered electronic imagers, e.g., charge-coupled device (CCD) cameras. However, one of the advantages of proton radiography is the capability of making "movies" of time-dependent phenomena at high frame rates (typically in excess of several megahertz) with many frames (23 frames of high-quality data are typically taken with the Los Alamos 800-MeV proton radiography system). Considerable effort has been devoted to developing detectors that can meet the requirements for frame rate, linearity, resolution, and dynamic range.

The FOM for radiography depends on both spatial resolution and intensity resolution. With an ideal detector these are determined by the proton optics and the Poisson statics of the transmitted proton fluence. Position resolution requires a detector system with small enough effective pixels in the image plane so the spatial resolution of the radiography is not compromised. The latter depends on the proton energy, the lens design, and the experiment. Current radiography systems require detectors with ~1000 × 1000 effective pixels mapped across the 12 × 12 cm^2 image plane.

Gated detectors

A proton detector converts protons into an electrical signal that can be digitized and recorded. In general this must involve at least one, and usually more, stages of amplification, g_i. It is desirable to have the noise introduced by the detector system be small compared to the Poisson statics of the proton fluence. The noise for a perfect amplifier is determined by the statistical fluctuation in the gain of each stage of the detector so that:

$$\frac{\delta I}{I} = \sqrt{\frac{1}{N}\left(1+\frac{1}{g_1}+\frac{1}{g_1 g_2}+\frac{1}{g_1 g_2 g_3}\ldots\right)} \qquad 11)$$

The dynamic quantum efficiency (DQE),

12)

$$DQE = \frac{1}{\left(1 + \frac{1}{g_1} + \frac{1}{g_1 g_2} + \frac{1}{g_1 g_2 g_3} \ldots\right)}$$

relates the image noise, $\delta I/I$, to the statistical noise of the transmitted proton fluence, N. It is clear from this expression that large gains, especially in the first stage, lead to a small impact of the detector on the image noise levels. This is important in the case where the image plane flux is limited.

The first optically shuttered proton radiography detectors developed for the 800-MeV LANSCE facility used a 2-cm-thick plastic scintillating plastic fiber bundle to convert the proton image to a light image. The light was focused using commercial lenses onto an array of four gated, cooled, 16-bit CCD cameras. A schematic of the optics is shown in Figure 4.

Each camera captured one image. Four cameras in the array allowed four images to be obtained each at different times. Fast gating was provided by applying 300- to 500-ns-long 12-kV pulses to custom 25-mm-diameter proximity focused planar diodes fiber coupled to the cooled CCDs. The planar photodiodes provided good linearity over several orders of magnitude.

An example of data taken with this system is shown in Figure 5. This is one frame from a sequence of flash radiographs taken of a detonation front moving through a high explosive puck. The frame

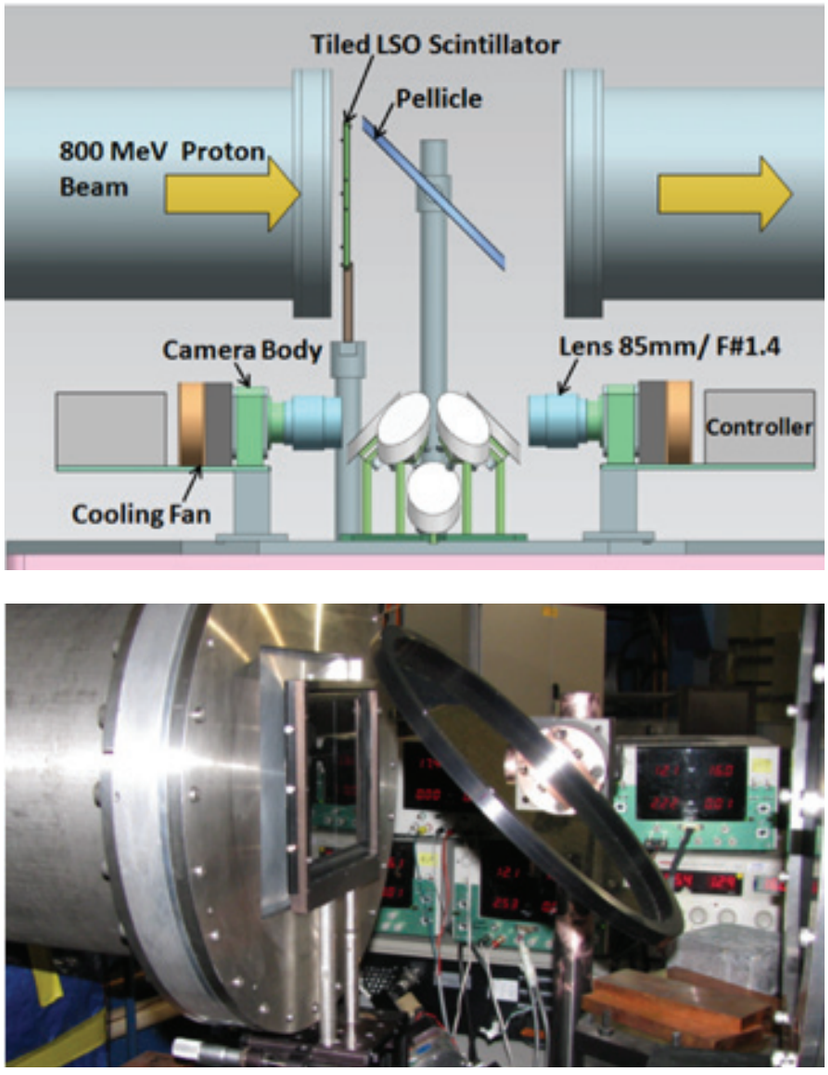

Figure 4. Top) Schematic of the light optics. Bottom) Photograph of the first proton radiography camera system.

rate was 10^6 Hz. Here the framing time was established by the width of the beam pulse to be 60 ns. The DQE of this system was measured by taking several beam pictures and measuring the standard deviation over a number of pixels. The data were rebinned to ensure the point-spread function of the optics did not influence the results. The DQE was calculated as:

$$DQE = \frac{X^2}{pixel} = \frac{\sum_{i-1}^{n} \frac{(n1_i - n2_i)^2}{n1_i + n2_i}}{n}. \qquad 13)$$

Here $n1_i$ and $n2_i$ are the number of protons incident on pixel i from two consecutive images, and the sum runs over n pixels. This expression assumes the pixels are independent of each other. Independence was determined by rebinning the data until a stable result was obtained.

The relatively low light output from the plastic scintillator coupled to the low quantum efficiency of the photocathode of the diode resulted in a system that had a DQE of ~30%. Flash proton radiography using 800-MeV protons is typically flux limited. This makes higher detector DQE desirable.

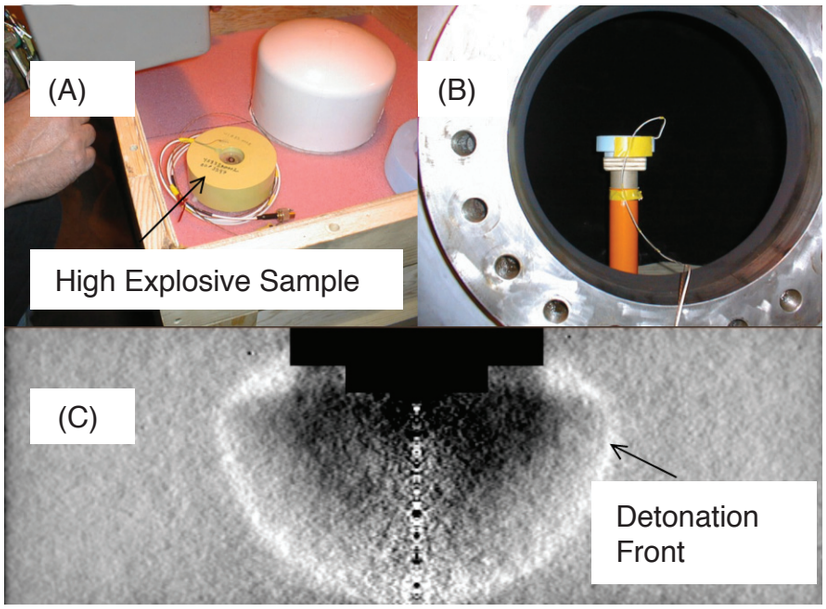

Figure 5. An example of data taken with a planer diode gated CCD camera viewing a PBX9502 high explosive sample. (A) shows the sample; (B) shows a side view of the sample mounted in the containment vessel; and (C) displays the result of an analysis of the change in the density, shown the detonation front in the sample. The exposure time was 60 ns and the fluence was 2 × 10^9 protons.

The path to higher DQE is to increase the front-end gain as shown by equation 12 (the scintillator gain and the quantum efficiency of the first stage of the detector).

Improved LANSCE detector

The pRad team continues to work to improve the performance and the DQE using indirect detection, where light from a scintillator screen in the image plane is optically relayed to a gated camera system. Two methods for improving the DQE are increasing the brightness of the scintillator screen and increasing the quantum efficiency of the stage that converts light to electrons. Both of these increase the first stage gain of a scintillator base detector.

A 720 × 720 pixel hybrid complementary-symmetry metal–oxide–semiconductor (CMOS) imager has been developed to provide higher quantum efficiency by eliminating the photocathode stage in the diode gate in the previous imager. These cameras are each capable of storing three frames of data in on-chip capacitive storage. The minimum gate width is ~150 ns and the minimum gate separation is ~250 ns. The framing time for proton radiography is determined by the proton pulse width. Since multiple detectors (7) view the radiation-to-light converter, adjacent frames can be taken on alternate cameras, so that data can be taken at frame rates up to 5 MHz.

The photo-sensor of the camera is a back-illuminated 720 × 720 pixel array of diodes fabricated in 100-µm-thick n-type silicon. Since the absorption length in Si, for lutetium oxyorthosilicate (LSO) generated 415-nm light, is about 200 nm most of the electron-hole carriers are created close to the back surface (n+-side of the sensor), where the electric field is the weakest. The dominant transport is thus that of the holes, which drift to the p-n junction at the interface to the CMOS Read-out Integrated Circuit (ROIC). The transit time for the holes at room temperature, at the nominal bias of 15 V is ~14.5 ns. This carrier transit time will affect how well the leading edge of the shutter gate is defined. The effect can be especially relevant when a photon pulse reaches the detector shortly before the shutter "turn-on time." The extinction ratio for pulses, which arrive at least 40 ns before the global shutter leading-edge, and also after the falling edge is very good, >4000:1. The extinction ratio is significantly better than what is observed in many fast monolithic CMOS cameras, especially for the light pulses arriving after the closing of the electronic shutter. This comes about because in the pRad camera the signal storage is done in metal-insulator-metal capacitors, and also because of the hybrid architecture of the FPA. The processed signal is stored outside the active silicon layer of the CMOS ROIC, and in addition the thick silicon detector acts as an effective light shield for the ROIC circuitry located underneath it.

Several options for radiation-to-light converters exist for the LANSCE imaging system. Several different tiled LSO systems can be used depending upon the experiment. LSO has the feature of fast response (40 ns), high light output (25,000 photons/MeV), and high density and, therefore, high light output in a given thickness. These properties allow the radiation-to-light converter to be a thin (2.5 mm) monolithic slab, rather than the 20-mm-thick fiber bundle that was used to get sufficient light with a plastic scintillator. The use

of a monolithic scintillator has eliminated an occasional problem of aliasing the fibers when small changes in position between calibration and dynamic images were introduced by the pressure pulse from the high explosives. The requirement for LSO with a minimum of light-scattering defects and the maximum available boule size limits the available scintillator size. Tiling is necessary to fully cover the 12 × 12-cm image plane and different configurations are used to ensure tile boundaries do not fall in a crucial place for a given experiment. The DQE of the camera system (LSO + hybrid CMOS detector) has been measured using the fluctuation technique described above and found to be 70(5)%, a large improvement of the CCD-based system. A major contributor to the reduction of the DQE from 100% is the read noise in this prototype system.

The use of scintillators coupled to cameras has reduced, but not eliminated, the problem of fluctuations induced by hadronic interactions in the detection system. In dynamic experiments at LANSCE, hadronic interactions in the photo sensor induce fluctuations, overwhelming the data in perhaps 1% of the pixels due to stray radiation interacting in the silicon. Median filtering replaces the data in the affected pixels for dynamic experiments. One CMOS camera feature is that it is only impacted by these "star" events while the gate between the sensor and the storage capacitor is on. This feature has eliminated stars for a number of experiments where MHz time response is not required. This has been accomplished by using a cesium iodide (CsI) radiation-to-light converter and only gating the camera to be on after the beam is off. Although the first 100 ns of light from the scintillator is discarded, the 1μs time response ensures sufficient light to obtain a high DQE, and the images are free of stars.

A new camera under development will provide 10 frames per camera, 1100 × 1100 pixels, a factor of 2 shorter minimum inter frame time and gate width, and a factor of 3 lower electronic noise. This new camera system promises more flexibility in the timing format, lower noise, and more frames. A variant of this design, which will provide 2000 × 2000 pixels, two frames, improved optical shuttering and lower noise, is also under development.

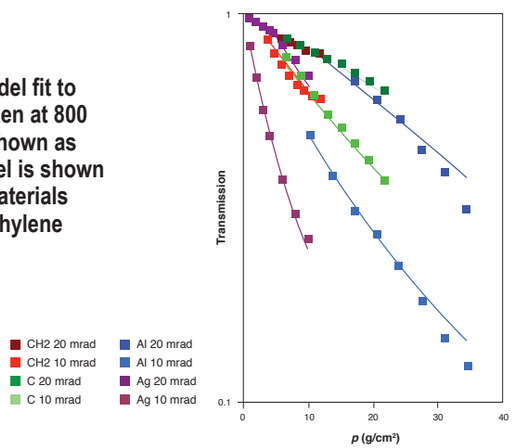

Figure 6. Global model fit to step wedge data taken at 800 MeV. The data are shown as points and the model is shown as a solid line for materials ranging from polyethylene (CH2) to silver (Ag).

Analysis and measurements

The effects of beam emittance and overburden material (windows, air, etc.) on the transmission can be included in the transmission model given earlier by adding the additional contribution to the beam divergence referenced to the target location, a, normalized to units of κ, in quadrature to the multiple scattering caused by the object. This gives:

$$t = e^{-\frac{l}{\lambda\theta}} \frac{1 - e^{-\frac{\kappa}{l+a}}}{1 - e^{-\frac{\kappa}{a}}} \qquad 14)$$

In this expression, the denominator accounts for the attenuation of the beam due to emittance and overburden when there is no object, and N_0 is measured in the object plane of the lens. The relationship between the divergence of the beam, θb, and the parameter a is:

$$a = \frac{X_0}{2}\left(\frac{\theta_b p\beta}{14.1\,\text{MeV}}\right)^2 \qquad 15)$$

If λ_θ and X_0 are treated as empirical parameters–good fits to transmissions–a function of thickness can be obtained.

Equation 14 can be inverted to obtain areal densities from experiments where the details of the object are not known. If care is taken to account for backgrounds, overburden materials, and position blur, it is possible to perform sub-one percent radiography using proton beams.

Photograph of the experimental area of the LANSCE Proton Radiography Facility.

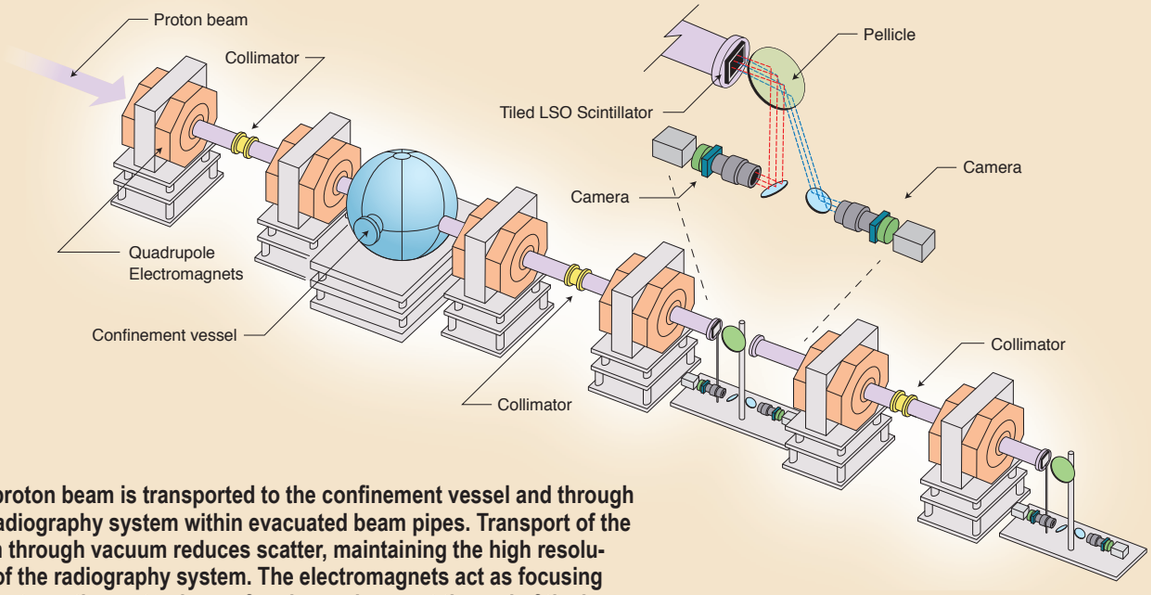

The proton beam is transported to the confinement vessel and through the radiography system within evacuated beam pipes. Transport of the beam through vacuum reduces scatter, maintaining the high resolution of the radiography system. The electromagnets act as focusing elements on the proton beam, forming an image at the end of the beam pipes in each of the air gaps. The protons interact with the scintillator material, generating a visible light image. This light is directed by mirrors to a series of cameras. Each fast-gated camera collects the light from a single pulse of protons. By combining these images into a time series a radiographic movie is formed of a dynamic event. Two magnetic lens systems are used to form two images, allowing additional frames to be added to the radiographic movies.

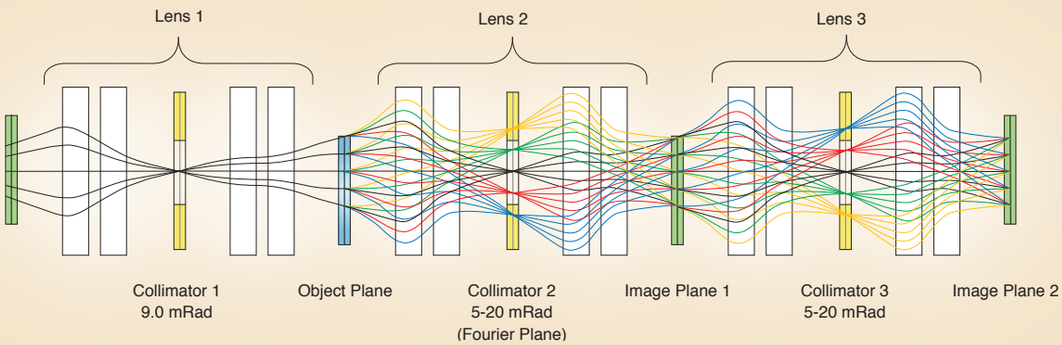

The black and colored lines represent trajectories of protons as they pass through the radiography system. The white boxes represent the quadrupole magnets, yellow boxes show the location of collimators, the blue box shows the object location and the green boxes represent the location of the proton images. The collimators are located at Fourier planes, where the extent of scattering within the object is mapped to radial position. Collimators, which consist of 18 inches of steel with an aperture machined along the beam axis, are located at these positions to remove protons that are scattered to large angles while letting pass protons that are only scattered to small angles. Small aperture collimators are used to radiograph thin objects while larger collimators are used for thicker objects. The protons that pass through the collimators are focused to proton images at the image planes, where scintillators are used to convert the proton image to a visible light image. The thickness of the object can be calculated from the light intensity of the collected images.

pRad at work

Proton radiography: A tool for solving complex problems in dynamic physics

The Proton Radiography (pRad) Facility at the Los Alamos Neutron Science Center (LANSCE) is a physics tool that can be applied to complex problems in dynamic environments. Its 800-MeV proton source penetrates through dense objects to reveal the intricacies of material behavior under extreme pressure-loading conditions. In contrast with x-radiography, its positively charged proton beam can be manipulated with electromagnetic lenses to eliminate parallax effects in the object plane by forming a plane wave proton pulse, much like an optical lens manipulating photon beams. In the interaction (object) region, the 800-MeV protons lose energy passing through dense objects, however, that leads to some blur (depending on the energy loss), in the image plane. Nevertheless, the tool reveals dynamic material properties with resolutions of ~6 line-pairs (LP)/mm, in contrast with most x-radiographic imaging systems of 3-4 LP/mm.

In one type of dynamic experiment, the pRad tool has been used to develop physics-based ejecta models for shock-loaded metals[1]. These physics and engineering models are being developed and implemented in hydrodynamics codes to better understand the dynamics of material failure of shock-loaded materials as the shock waves reach and reflect from the metal-vacuum interface of shock loaded materials. The basic geometry from this work, the concept, and two pRad images are seen in the figure on the next page.

This figure presents a snapshot of unstable Richtmyer-Meshkov (RM) growth of solid and liquid metals in vacuum[1]. The metals were (high) explosively (HE) loaded by detonation of a 76-mm-diameter plane wave lens used to initiate other explosives such as a TNT or PBX 9501 booster. The TNT-type explosives were used to drive a shock wave into Sn, causing the Sn to liquefy and the surface perturbations to unstably grow. The PBX 9501 was used to shock OFHC Cu. In the Sn case the goal was to validate the applicability of RM physics to ejecta formation from roughened surfaces as the shock waves interact with the surface perturbations or scratches. In the Cu case researchers were evaluating the utility of RM physics to evaluate material strength at high strains and strain rates.

Considering the figure in more detail, to the left is the notional geometry typically used in RM-physics experiments at the pRad facility. For example, researchers encase the 76-mm-diameter HE lens in acetal plastic to confine the explosion and maintain detonation pressures. The HE lens then initiates the HE booster (TNT or PBX 9501) that drives a shock wave into the target assembly. As illustrated in the center panel, the target has small sinusoidal perturbations on it that are characterized by wavelength, λ, and amplitude, $h_0/2$. As the mostly planar shock waves arrives at the interface it first releases to zero pressure at the perturbation minima and then reflects back into the metal as a rarefaction wave. A brief time later the shock wave releases to zero pressure at the perturbation maxima, also reflecting back into the metal as a rarefaction wave. Under these conditions, the stresses produced by the shock wave interacting with the perturbations cause the perturbation minima to compress, invert, and then grow in tension as RM instabilities (spikes) into vacuum. Because the compressed RM spikes grow quickly relative to the initial perturbation maxima, the initial maxima invert

and form bubbles that unstably grow into the metal causing metal to flow into the spikes to support the spike growth. In this picture, bubbles and spikes refer to peak penetration depths on the opposite sides of the free-surface, which is nominally defined as the plane through the inflections of the initial two-dimensional sinusoidal surface perturbations. Importantly, the shocked free-surface will have a particle velocity caused by the impulse that is related to the strength of the impulse. The bubbles grow in a negative sense into the metal (Sn or Cu) relative to the free surface, and the spikes grow in a positive sense relative to the free surface. Thus, there are three velocities that are important: the bubble, the free-surface, and the spike velocities. These physics are notionally illustrated in the center panel. The final panel shows one snapshot of each the Sn and Cu from two pRad experiments. These target assemblies had wavenumber amplitude products of $h_0k \in \{3/4, 1/8, 3/8, 3/2\}$ from the top in the figure. Clearly evident are bubble and spike dynamics for the h_0k products in the Sn and Cu. The images to the right in the figure were acquired 7.7 μs after the shock wave reached the Sn/Cu interface. The shock wave pressures for the two geometries were 210 kbar (21 GPa) for the Sn, and 360 kbar (36 GPa) for the Cu. The free-surface and spike velocities can be estimated from the image time (7.7 μs), and the distance the surface and spikes have traveled. Full documentation of these experiments is in the reference below[1].

The goal of the Sn work was an ejecta model based on RM physics. That model is represented by Eqs. 2.1 to 2.9 in the reference below[1]. The Cu data evaluated an idea developed by Piriz, et al.[2]. In that work, they postulated that the growth and arrest of surface perturbations in shocked metals that were solid on shock and release could be used to estimate material strength. In applying their ideas Los Alamos researchers estimate the material strength of Cu from the $h_0k = 3/8$ perturbation region of Cu to be about 0.5 GPa[1]. The idea is to look at perturbations that invert, grow, and then arrest. It is seen that for $h_0k = \{3/4, 3/2\}$ that the instabilities grow without bound, like the liquefied Sn. In this case they have formed ejecta. When the growth begins and then arrests the velocimetry contains information about material strength. Laboratory researchers are currently exploring these types of Cu data further with simulations and strength models, such as PTW[3], and hope to report on that work soon.

[1] W. T. Buttler, et al., "Unstable Richtmyer-Meshkov growth of solid and liquid metals in vacuum," *J. Fluid Mech.* **703**, 60-84 (2012).

[2] A. R. Piriz, J. J. Lopez-Cela, N. A. Tahir, and D. H. H. Hoffmann, "Richtmyer-Meshkov instability in elastic-plastic media," *Phys. Rev. E.* **78**, 056401 (2008).

[3] D. L. Preston, D. L. Tonks, and D. C. Wallace, "Model of plastic deformations for extreme loading conditions," *J. Appl. Phys.* **93**, 211-220 (2003).

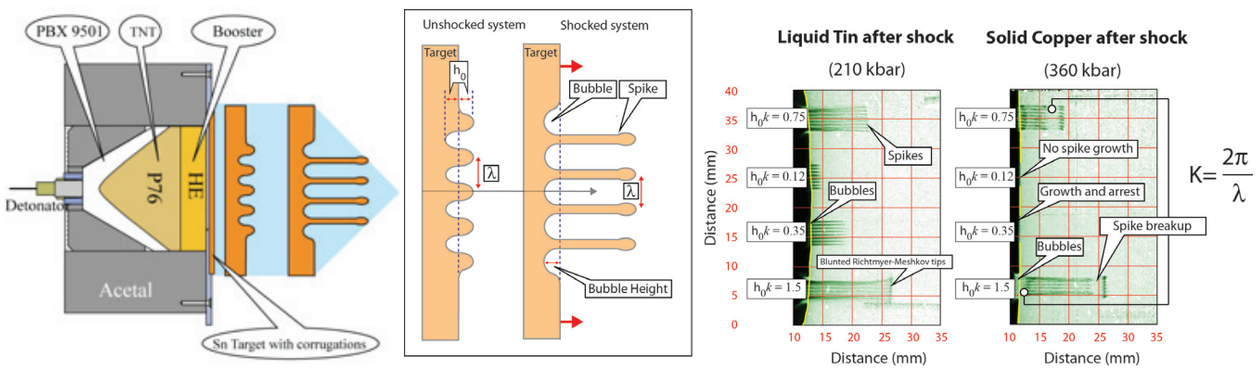

The left figure approximates typical experimental geometry, in which an HE booster is initiated with a 76-mm-diameter HE lens. The sample surface has sinusoidal perturbations defined by their wavelength (λ) and amplitude (*h*), as shown in the middle figure. The pRad proton beam is aligned along the perturbations to image the unstable Richtmyer-Meshkov flows, as shown in the pRad images to the extreme right. The perturbations are characterized by the wavenumber (k = 2π/λ) amplitude products (h_0k), and the growth rates are higher for larger h_0k.

Broader exposition of the utility of pRad for DoD programs

The Proton Radiography (pRad) Facility at Los Alamos National Laboratory's Los Alamos Neutron Science Center (LANSCE) offers a unique capability that supports developing a better understanding of such problems as failure of materials due to shear band formation, spallation, crack propagation, solid-solid phase transitions, and change in density of materials. Many of these problems are concomitant with the evolution of dynamic deformation occurring under impact of a shape charge jet, kinetic energy impactor, or any other loading condition. The Department of Defense (DoD) and the U.S. Army Research Laboratory (ARL) have a pressing interest to understand the evolution of phenomena under dynamic-loading conditions and also the end state attained at the termination or cessation of the dynamic event.

The uniqueness of the Laboratory's pRad facility for meeting the needs of DOD/ARL stems from the following two factors:

1. With a relatively long mean free path and high spatial resolution (200 μm x 200 μm) of the 800-MeV protons, pRad is well suited to study dynamic interactions within large volumes of materials of interest to DoD/ARL. This allows for problems, such as characterization of deformation processes dependant on effects of inertial material confinement and deformation processes within complex systems of materials, to be studied directly in situ, instead of indirectly and piecewise.

2. pRad provides an accelerator-based cineradiography diagnostic, which has the capability of capturing multiple radiographs throughout a dynamic event, recording the evolution of density sensitive phenomena, including the recovered end-state of the process. The integration of proton cineradiography with the capability to impart dynamic loads, through gun-accelerated impacts, shaped-charge jet penetration and high-explosive detonations, further expands areas of interest to DoD/ARL.

These factors motivated ARL scientists to initiate a study at the Los Alamos Proton Radiography Facility to simultaneously investigate the compression of a material and the associated penetration dynamics at extreme pressures. Figure 1 shows a radiograph acquired some time after a metallic jet impacted a target from one experiment. Future experiments can probe the evolution of material deformation and failure due to impact of a kinetic energy projectile striking armor material, including the final end state attained in the armor material (Figure 2). Similarly, the pRad facility could be used to characterize the deformation modes and mechanisms of composite materials such as those that occur when a bullet strikes a helmet (Figure 3). Such an experiment at the pRad facility is expected to yield information about the deformation mechanisms within the composite as well as provide ancillary information on the deformation of the internal surface, which ultimately may provide valuable clues to prevent trauma suffered by the warfighter.

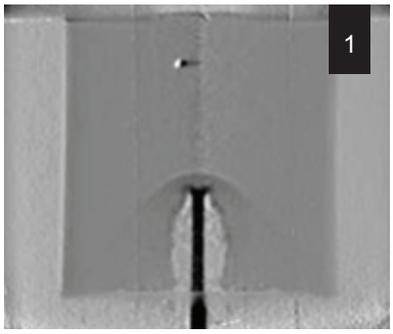

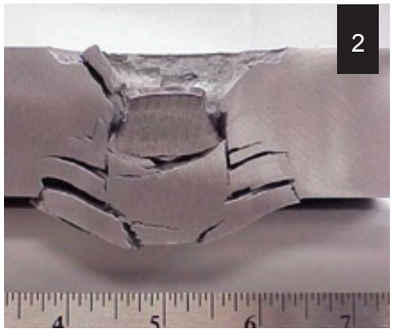

Figure 1) Proton radiograph of a jet penetration (penetration direction bottom to top). Figure 2) Optical photograph of an armor material cross section acquired after impact of a kinetic energy projectile (impact direction top to bottom). Figure 3) Optical photograph of a composite material helmet just prior to a kinetic energy projectile impact (projectile moving from right to left).

Predicting plastic deformation of metals using large-scale hydrodynamic simulations

Numerous defense applications rely on the ability to predict the plastic deformation of metals using large-scale hydrodynamic simulations. These simulations utilize embedded constitutive models describing the continuum-level strength of the material. The strength model parameters are primarily obtained through the fitting of stress-strain curves obtained from quasi-static load frames and Hopkinson bar experiments.

As such, both the strength models and the simulations that rely on them are most accurate throughout the range of conditions where these experimental techniques are well suited to yield data: strains <100% and strain-rates $<10^4$ s^{-1}.

However, defense applications such as explosive loading and high-velocity impact often reach conditions with strains of several hundred percent at strain rates between 10^5 s^{-1} and 10^8 s^{-1}. The validity of strength models at these more extreme conditions is currently being assessed using experiments that generate and measure

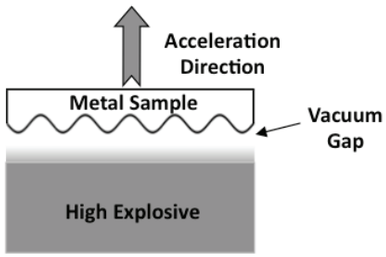

strength-inhibited Rayleigh-Taylor (RT) instability growth in metals.

Recently, a series of experiments to measure RT instability growth in solid metals, building on the techniques originally developed by Barnes, et al.[1], have been conducted at the Proton Radiography (pRad) Facility at the Los Alamos Neutron Science Center (LANSCE). The experimental technique utilizes the by-products from a high-explosive plane wave lens to shocklessly accelerate a sample with a sinusoidal perturbation imposed on one surface.

pRad is used to measure the growth rate of the unstable perturbations as a function of time by acquiring 20 to 40 radiographs of each experiment with a temporal spacing of 350-500 ns and a spatial resolution of ~100 μm. A representative proton radiography data set is shown below in which an annealed copper sample was perturbed with an initial sinusoidal perturbation 2.0 mm in wavelength and 55 μm in amplitude. The high explosive by-products reached the perturbed surface of the sample and began to accelerate it 6.9 μs after the experiment was initiated.

Analysis of each proton radiograph yields the peak-to-trough perturbation amplitude at each image acquisition time. These amplitudes are compared to the perturbation amplitudes predicted using different strength models in hydrodynamic simulations. Variation of sample material, acceleration, and the initial perturbation amplitude allows assessment of the predictive accuracy of strength models under these high-strain and strain-rate conditions.

[1]Barnes, J.F., et al., *J. Appl. Phys.* **45**, 727 (1974).

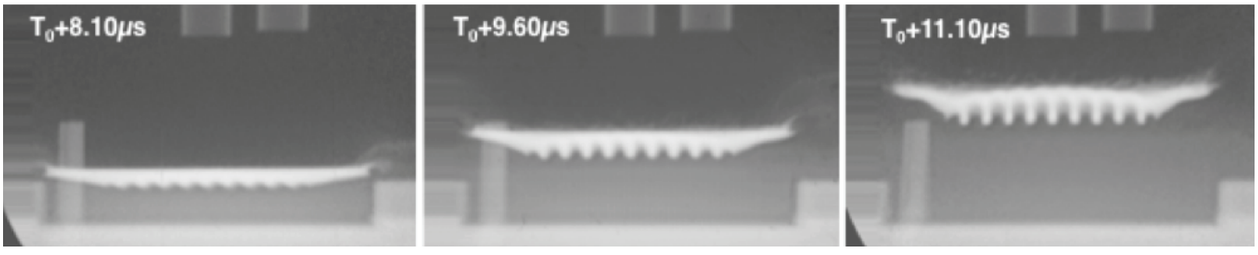

Representative proton radiography time sequence in which an annealed copper sample was perturbed with an initial sinusoidal perturbation 2.0 mm in wavelength and 55 μm in amplitude and then driven by expanding detonated HE by-products.

In situ monitoring of dynamic phenomena during solidification

The creation of microstructures by design with application-tailored properties requires directed synthesis and processing. Los Alamos National Laboratory scientists and collaborators are developing methods to monitor dynamic phenomena directly during phase transformations at non-ambient temperatures using novel imaging techniques. This will enable control of microstructure evolution, will allow for the validation and advancement of science-based theories, and will enable predictive model development over the length scale relevant for phase transformations and microstructure evolution.

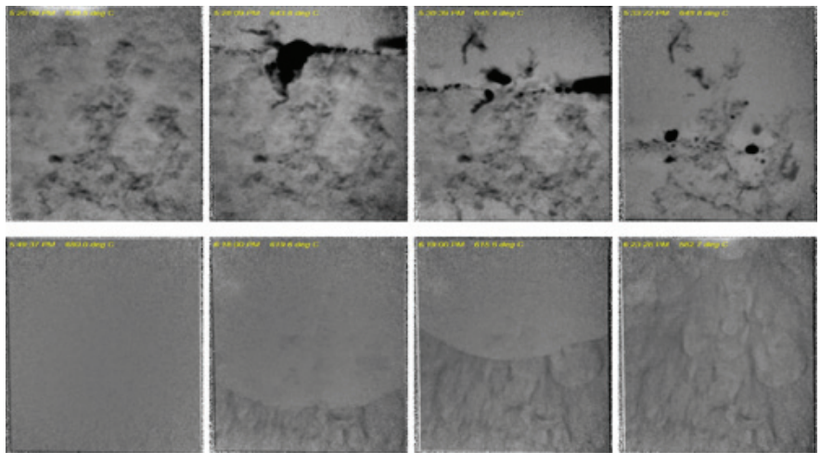

Time-resolved pRad images obtained during melting from the top downward (upper row images) and directional solidification from the bottom upward (lower row images) of a bulk 6-mm-thick aluminum-indium sample. The field of view is approximately 44 x 44 mm^2. The darker regions observed during melting are indium-rich liquid, consistent with the liquid-liquid phase separation anticipated at elevated temperatures for this alloy system.

Metallurgy (MST-6) researchers and the Proton Radiography team completed the first in situ examinations of melting and solidification in aluminum-indium, gallium-bismuth, tin-bismuth, and aluminum-copper alloys using 800-MeV proton radiography (pRad). A unique capability at the Los Alamos Neutron Science Center (LANSCE), pRad probes dynamic material phenomena.

In this new application of pRad for materials studies, the researchers imaged heating and cooling of bulk metal alloy sections ranging from 2 to 6 mm in thickness (see figure). These images highlight liquid-liquid phase separation at elevated temperatures and solid-liquid interface movement. Advantages of proton radiography for these experiments include the following:

1. time-resolved imaging of dynamic phenomena (e.g., localized fluid flow and solute segregation during solidification) and microstructure evolution,

2. examination of a large field of view in millimeter-thick samples (relevant to casting) that enables bulk materials analysis, and

3. the ability to examine high density materials.

The in situ methods will enable tomographic studies of 3D microstructure evolution during processing. The monitoring techniques will help to achieve transformational advances in the creation of microstructures by design, which has been identified as a key grand challenge for synthesis and processing materials science. Moreover, this work will help to define key MaRIE capabilities needed for future process-aware solidification studies at Los Alamos. MaRIE (for Matter-Radiation Interactions in Extremes) is the Laboratory's proposed experimental facility for the discovery and design of advanced materials.

Using proton radiography to study penetration dynamics

U.S. Army Research Laboratory (ARL) scientists recently began utilizing the Los Alamos National Laboratory Proton Radiography (pRad) Facility to simultaneously study compression of a material and associated penetration dynamics at extreme pressures. The study consisted of observing a metallic jet penetrating a cylinder of armor material at the pRad facility. The goal of this study was to gather high-resolution, time-sequenced information essential for understanding how a current armor material's physical mechanisms enhance penetration resistance during jet interactions. The figure below shows a time-sequential series of radiographs acquired just after the metallic jet impacted a target from one experiment.

In this experiment, radiographs provided information about the jet penetration rate, jet erosion dynamics, target material deformation, and the penetration cavity evolution. The relatively long mean free path of 800-MeV protons, combined with a 120-mm x 120-mm imaging window, allowed material density measurements with sufficient contrast in targets where geometry provided some level of inertial confinement. Using static radiographs, the density of nominal material was measured to within 4% of the absolute material density. Because of pRad's unique capability to measure absolute material density at numerous times, ARL scientists were able to study the evolution of the three-dimensional compression front (often referred to as a Mach cone) from impact, throughout its development, to its relatively steady state structure. This relatively steady state structure becomes established after ~5 μs of penetration for the material studied. Density measurements made within the steady state region directly ahead of the jet revealed the highest densities. In this region, the measured value of the density is found to be significantly different from both density measurements made quasistatically using diamond anvil cells (DAC) and dynamically from uniaxial compression plate impact experiments at similar pressures. Absolute material density measurements from proton radiography during the penetration event indicated that, when probed dynamically with a jet, the armor material specimen compressed only to ~70% of the density that would be expected when applying material equation of state derived from quasistatic DAC and plate impact experiment measurements. Since theories of penetration mechanics are contingent on the penetrating medium's compressibility, deformation response, and ultimate density, a clear understanding of the in situ material response (i.e., the observed discrepancy in density) is important for designing armor with a high penetration resistance.

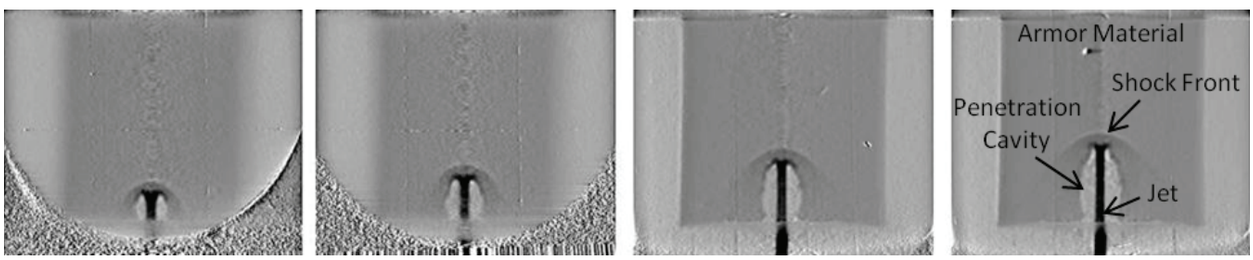

Movie of a metallic jet penetrating into a cylindrically shaped armor material. Time increases from the left image to the right image.

pRad into the future

3-GeV proton radiography

Mission need

Future certification of nuclear weapon systems will require a predictive understanding of dynamic materials response within simulations of full-scale weapons systems. These simulations will rely on accurate constitutive models (i.e., continuum rather than molecular dynamics models) of material dynamics at the component level. The validation of these models will require state-of-the-art imaging of small- to medium-scale experiments. Ideally, these experiments will be executed at an upgraded Proton Radiography (prad) Facility at the Los Alamos Neutron Science Center (LANSCE), which would provide multiple-time radiography with unprecedented spatial, temporal and density resolution.

Once these macroscopic models are developed and validated at the component scale, full system simulations will be validated through hydrodynamic experiments, which are ideally executed at the Dual Axis Radiographic Hydrodynamic Test Facility (DARHT).

The Multi-Probe Diagnostic Hall (MPDH) has been proposed as part of MaRIE, the Matter-Radiation Interactions in Extremes experimental facility, for material dynamics studies at very small length scales in small-scale experiments as a means to provide an understanding of material behavior at a fundamental level. The insights provided by this fundamental understanding must then be extrapolated to inform the development of improved constitutive models of macro-scale systems. An upgraded proton radiography capability at LANSCE, partnering with the MPDH experimental program, provides an excellent experimental capability to test and guide the extrapolation of the micro-scale models developed at MaRIE to the larger scale required for weapons certification.

An enhanced proton radiography capability, which can probe sub-grain length scales of macroscopic objects with sub-percent density resolution, is required to study the full spectrum of component-level material science that will challenge the future nuclear weapons program. A proton beam energy increase from 0.8 GeV to 3 GeV and a beam current increase from 3 x 10^8 to 1 x 10^9 protons/micro-

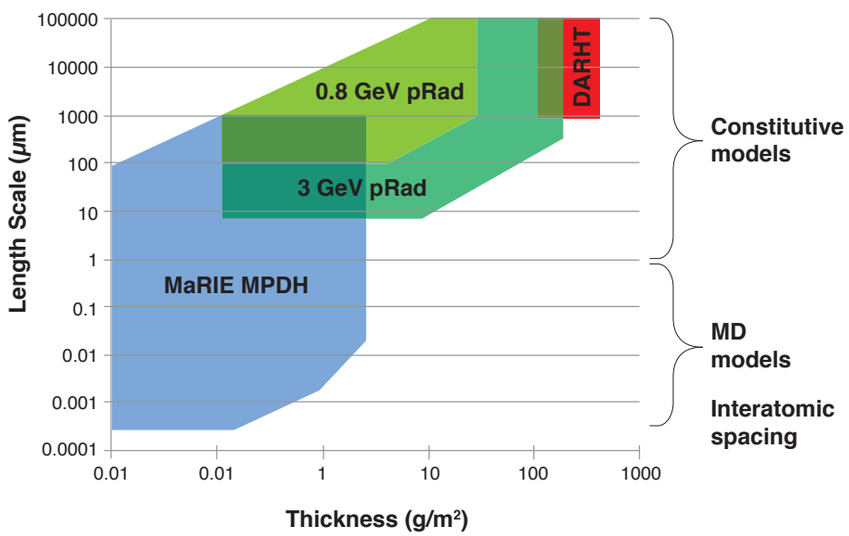

Figure 1: The object thickness and length scale regimes to be studied at DARHT, 0.8-GeV pRad, 3-GeV pRad, and high-brightness light sources such as proposed at MaRIE. The high-brightness light sources of MaRIE provide the fundamental understanding of material dynamics at the smallest length scales, while DARHT studies full-system primary performance. The proposed 3-GeV pRad facility fills the gap between these experimental capabilities with constitutive model validation at the component level.

pulse will provide the required spatial and density resolution through a large range of objects, as well as allow measurements of hazardous materials properties, such as plutonium and beryllium, which require secondary containment.

The increased proton energy and current combined with a new imaging system optimized for 3-GeV radiography, will provide spatial resolution of ~10 microns for small, thin objects and provide high-resolution (<300 microns) radiographs of relatively thick objects (up to 150 g/cm^2). Figure 1 shows the regions in resolution-areal density space that MaRIE, DARHT, and the enhanced Proton Radiography Facility will study. High-brightness light sources such as those proposed at MPDH will focus on the shortest length scales and the smallest objects, DARHT will test the larger length scales of the thickest objects, and a 3-GeV pRad capability will study mid-scale objects in the intermediate regime. These three facilities working together will provide a solid wealth of knowledge covering the full range of scales—from atomic to complete assemblies—to characterize and certify nuclear weapons systems and address new challenges as they arise.

Facility description: 3 GeV, 30 mA LANSCE Accelerator Enhancement

The development of new accelerator and beam transport technologies in the past 40 years allows the improvements described above to fit into the existing infrastructure at LANSCE. This means that the proton energy can be increased to 3 GeV and the beam current can be increased by a factor of 3 within the existing conventional facilities (accelerator tunnel, equipment buildings, site power, and experimental facilities).

Presently, LANSCE accelerates and delivers beam through room-temperature structures. Replacing some of these with superconducting radio-frequency (RF) structures allows for higher acceleration gradients, and higher field dipole magnets can achieve the larger fields required to bend higher energy protons within the existing tunnel structures. The radio-frequency quadrupole is now a standard accelerator technology and can be used at the low-energy end of the LANSCE accelerator to increase the current that can be delivered to the Proton Radiography Facility.

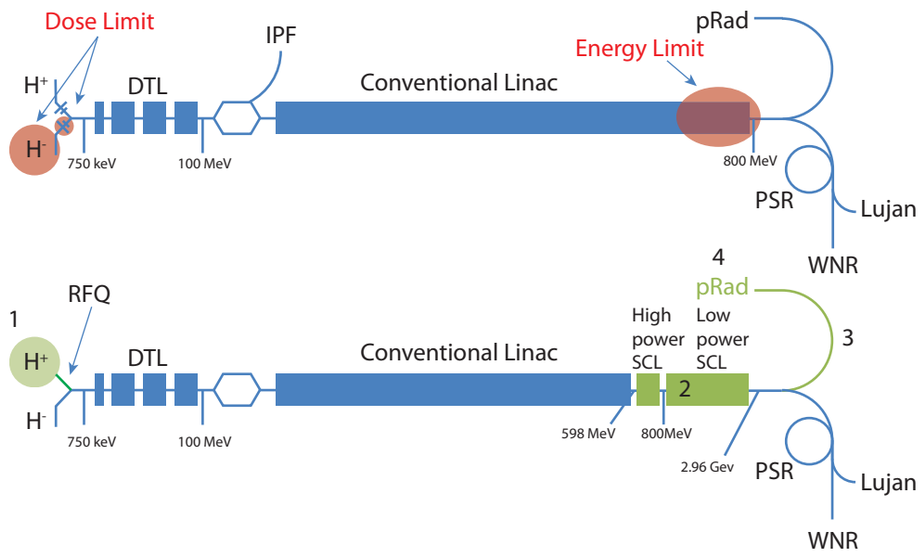

Figure 2: Top: Layout of the existing LANSCE facility with injectors at the left and experimental areas at the right. The red regions are the location of the present beam current (or dose) and energy limitations. Bottom: The modifications that allow the delivery of 30-mA peak current at 3 GeV. Instead of the existing H- source, a high current H+ source and RFQ would inject into the linac. The last two sectors of conventional RF would be replaced with superconducting RF. The RF beyond the 0.8-GeV cavities would be de-energized while the 0.8-GeV beam is delivered and the low-power superconducting RF would be re-energized when the 3-GeV pRad beam is required. Numbers in the lower picture correspond with item numbers in the text on the next page.

Los Alamos National Laboratory has completed feasibility and technology trade studies of a 3-GeV upgrade to the LANSCE Accelerator. One ground rule for this study was to leave the existing LANSCE capability intact, allowing continued delivery of 0.8-GeV protons to the Lujan Neutron Scattering Center as well as the Weapons Neutron Research Facility and 0.1-GeV protons to the Isotope Production Facility. The resulting conceptual design requires the replacement of four major components of the LANSCE facility as shown in Figure 2.

1. Install a high current H+ (proton) source, beam chopper, and 750-keV RFQ injector to gain the increased current.
2. Replace the final two sectors of the existing accelerator with high-gradient superconducting cavities capable of accelerations up to 3 GeV (switchable for high power RF to 0.8 GeV and low power RF to 3 GeV).
3. Replace the 0.8-GeV beam transport system from the linac to Area C, where the existing pRad capability is located, with a 3-GeV proton transport line.
4. Replace the existing radiography system in Area C with an optimized 3-GeV imaging system.

The accelerator enhancements described here will take full advantage of the existing infrastructure as well as build on the ongoing linac risk mitigation efforts. For example, the linac risk mitigation effort plans to invest in 201-MHz and 805-MHz RF power supplies for the existing, normal-conducting accelerator. These same power supplies will be utilized in the linac enhancements proposed here. The 201-MHz RF power supplies will continue to be used to accelerate beam in the drift-tube linac accelerator, and the 805-MHz klystrons, which will also be provided as part of the linac risk mitigation effort, would be used to energize the super conducting structures. Because of the increased efficiency of superconducting cavities these same RF power supplies will be able to accelerate the beam up to 3 GeV.

Next Generation Proton Radiography Detector

Neutron Science and Technology (P-23), with Teledyne Scientific and Imaging, is leading the development of the Next Generation pRad (proton radiography at the Los Alamos Neutron Science Center) Detector. The Fast Mega-Pixel Burst Mode Imager for Multi-Frame Radiography will deliver increased special and temporal resolution, expanding the capability for essential radiographic capabilities at the pRad facility. Cameras will employ complementary metal-oxide-semiconductor (CMOS) with a readout integrated circuit chip for the imager in a focal plane array. Following extensive efforts between P-23, the Physics Division Office, the Associate Directorate for Experimental Physical Sciences, the Science Campaign Program Director, and Procurements, the subcontract for the Phase 1 of the development was issued in 2010. Science Campaign C3 Advanced Radiograph and Transformational Technology and C1 Primary Assessment Technology are funding this development program.

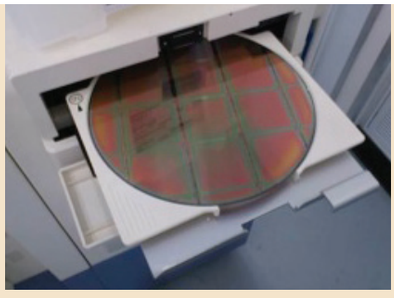

A 200-mm-diameter CMOS wafer at probe station at Femtotest.

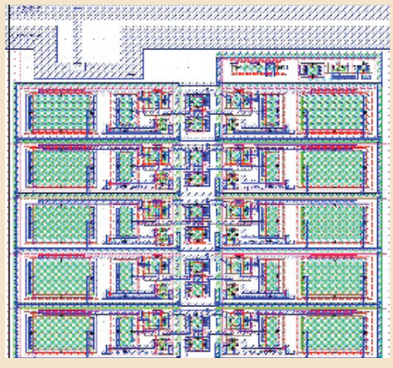

Ten-frame imager pixel layout; the 40-µm x 40-µm pixel shown above, in 180-nm CMOS process allows 10 signal storage capacitors per pixel.

Proton Radiography team: Back row (left to right); Robert King (P-23), Brian Hollander (P-25), Carl Wilde (P-23), Paul Nedrow (P-23), Kris Kwiatkowski (P-23), Jeff Wang (P-25): Middle row (left to right); Joel Heidemann (WX-3), Josh Tybo (P-23), Frank Merrill (P-23), Andy Saunders (P-25), Robert P. Lopez (WX-3), Matthew Murray (P-25), Camilo Espinoza (P-25), Gary McMath (WX-3): Bottom row (left to right); Wendy McNeil (WX-3), Julian Lopez (P-25), Jonathan Roybal (P-25), John Perry (ISR-1), Jason Medina (P-25), Amy Tainter (P-25), Heather Leffler (NSTec).

Proton Radiography team fires 500th shot

On January 23, 2012 the Proton Radiography (pRad) team fired pRad shot number 500. This landmark shot was the second member of the "High Explosive (HE) Gaps" experiment series. The series examines the initiation of insensitive high explosive across a vacuum-or matter-filled gap.

The first proton radiography shot was conducted on April 15, 1997, in beam Line B at the Los Alamos Neutron Science Center (LANSCE). In the intervening time, the team has recorded 45,111 proton pulse chains into 41,420 series of pictures, ranging from 4 pictures per series in the earliest days to as many as 2,000 pictures per series for the Moxie camera test shot and 5,000 for a typical cook-off experiment. The capability is 41 frames per series in typical modern running. Experiments have ranged in size from 100 miligrams to 10 pounds of high explosives, and have contained uranium, plutonium, xenon, and many other elements, with densities ranging from a few mg/cc to tens of g/cc. Secondary diagnostics have included VISAR (velocity interferometer system for any reflector); PDV (photonic Doppler velocimetry); temperature probes; visual framing cameras; and piezo, optical, and voltage pins.

The team is proud to have been able to make 500 contributions to the weapons program and is eager to continue for the next 500.

Funding sources include the NNSA Science campaigns, the Laboratory Research and Development program, Work-for-Others including Defense Threat Reduction Agency, Atomic Weapons Establishment, and Lawrence Livermore, Sandia, and Oak Ridge National Laboratories. The work supports the Laboratory's Nuclear Deterrence and Global Security mission areas and the Materials for the Future and Science of Signatures science pillars.

Acknowledgements
Eric Brown, William Buttler, Amy Clarke, Kris Kwiatkowski, Fesseha Mariam, Frank Merrill, Chris Morris, Russ Olson, Mike Zellner, and the pRad team in both Physics and Weapons Experiments Divisions.

Published by the
Experimental Physical Sciences Directorate

Editor: Karen Kippen
Designer: Jim Cruz
Copy Editor: Diana Del Mauro
Photographers: Ethan Frogget, Sandra Valdez

To read past issues of The Pulse,
see lansce.lanl.gov/pulse.shtml.

Physics

LANSCE
Los Alamos Neutron Science Center

Wendy McNeil prepares a shot prior to lifting the high explosives package into the containment vessel. The fibers are part of a photon Doppler velocimetry (PDV) system that is routinely deployed to measure the velocity of selected components of the shot.

Los Alamos
NATIONAL LABORATORY
EST.1943